TABLE OF CONTENTS:

COMPLETE AUTHOR LIST FOR SELECTED REFERENCES

Reference 1. Branton, D., Deamer, D. W., Marziali, A., Bayley, H., Benner, S. A., Butler, T., Di Ventra, M., Garaj, S., Hibbs, A., Huang, X., Jovanovich, S. B., Krstic, P. S., Lindsay, S., Ling, X. S., Mastrangelo, C. H., Meller, A., Oliver, J. S., Pershin, Y. V., Ramsey, J. M., Riehn, R., Soni, G. V., Tabard-Cossa, V., Wanunu, M., Wiggin, M., & Schloss, J. A. The potential and challenges of nanopore sequencing. *Nat. Biotechnol.* **26**, 1146-1153 (2008).

Reference 17d. Harris, T. D., Buzby, P. R., Babcock, H., Beer, E., Bowers, J., Braslavsky, I., Causey, M., Colonell, J., Dimeo, J., Efcavitch, J. W., Giladi, E., Gill, J., Healy, J., Jarosz, M., Lapen, D., Moulton, K., Quake, S. R., Steinmann, K., Thayer, E., Tyurina, A., Ward, R., Weiss, H., & Xie, Z. Single-molecule DNA sequencing of a viral genome. *Science* **320**, 106-109 (2008).

Reference 17e. Eid, J., Fehr, A., Gray, J., Luong, K., Lyle, J., Otto, G., Peluso, P., Rank, D., Baybayan, P., Bettman, B., Bibillo, A., Bjornson, K., Chaudhuri, B., Christians, F., Cicero, R., Clark, S., Dalal, R., Dewinter, A., Dixon, J., Foquet, M., Gaertner, A., Hardenbol, P., Heiner, C., Hester, K., Holden, D., Kearns, G., Kong, X., Kuse, R., Lacroix, Y., Lin, S., Lundquist, P., Ma, C., Marks, P., Maxham, M., Murphy, D., Park, I., Pham, T., Phillips, M., Roy, J., Sebra, R., Shen, G., Sorenson, J., Tomaney, A., Travers, K., Trulson, M., Vieceli, J., Wegener, J., Wu, D., Yang, A., Zaccarin, D., Zhao, P., Zhong, F., Korlach, J., & Turner, S. Real-time DNA sequencing from single polymerase molecules. *Science* **323**, 133-138 (2009).

METHODS AND MATERIALS

Experimental conditions for DNA polymerase binding and primer extension studies. In typical polymerase binding and primer extension experiments, KF(exo$^-$) (3'→5' exonuclease-deficient mutant of the Klenow fragment of *E. coli* DNA polymerase I) was added to a final concentration of ~7 nM after the formation of the rotaxane had been confirmed. Relatively low amounts of the required deoxynucleotide triphosphates (dNTPs, 20 nM of each type) were added to facilitate primer extension studies to promote distributive DNA polymerase action (one nucleotide per incorporation event). All experiments were conducted at room temperature (22 ± 2 ^{o}C) in a buffer solution containing 150 mM KCl, 25 mM Tris, 4.5 mM $MgCl_2$ at pH 7.5 if not mentioned otherwise. The *cis* side of the bilayer is defined as the ground regarding the sign of the applied potentials.

Data collection, processing, and analysis. Raw ion current recording was acquired at sample rates of 10 kHz or higher using an Axopatch-1D or 200B amplifier *via* a Digidata 1322A D/A converter. Data collection was done by the *Clampex 10.2* software. Data processing and DNA polymerase binding kinetics analysis was done by the *Clampfit 10.2* software. All instrumentation and software are products of Molecular Devices (Sunnyvale, CA).

Materials. All DNA polymerases were purchased from New England BioLabs Inc. (Ipswich, MA). The dNTP kit was purchased from Sigma-Aldrich (St. Louis, MO). The threading strand was made with an Applied Biosystems ABI 394 DNA/RNA Synthesizer (Foster City, CA) with standard phosphoramidite reagents purchased from Glen Research (Sterling, VA). DNA primers were custom made by e-Oligos (Hawthorne, NY). Details for the purification and characterization of the threading strand and DNA primers were performed as previously described (ref. 4). The lipid used in this study, 1,2-diphytanoyl-*sn*-glycero-3-phosphocholine, was purchased from Avanti Polar Lipids (Alabaster, AL) and the Teflon sheet supporting the formation of the planar lipid bilayer was a PTFE film with a thickness of 25 μm purchased from Goodfellow (Huntingdon, UK).

SUPPORTING DISCUSSIONS

- **Lifetimes (τ) derived from DNA polymerase - rotaxane interaction monitored at the single-molecule level (Table 1)**

The association and dissociation processes of the interaction between DNA polymerase and the rotaxane dsDNA segment are intrinsically dissected when they are monitored at the single-molecule level. In the context of our experiment, the ion current recording represent either the free dsDNA *"OFF"* state (baseline ion current level) or the DNA polymerase bound "*ON*" state (high ion current level), where each OFF state duration represents the *"waiting time"* before the next DNA polymerase association event, and vice versa (Figure 2a). An analysis can be performed to derive the lifetime (τ) of both association and dissociation processes when a statistically relevant number ($n > 30$) of single-molecule DNA polymerase binding events to the rotaxane dsDNA segment can be recorded. For example to obtain the association lifetime (τ_{ON}), the histogram for individual ON event durations was constructed, then fitted to an exponential decay function [$y = A_o exp(-t/\tau_{ON}) + C$] by non-linear regression. Histogram bin width (h) was determined using the Scott formula (ref. 15): $h = 3.5\sigma \times n^{-1/3}$, which is mathematically appropriated for displaying histogram distribution features (σ = standard deviation of the events of interest).

Lifetime (τ) and rate constant (k) have a simple reciprocal relationship. The former is derived from a collection of single-molecule events and the latter is an ensemble level description of the DNA polymerase kinetic property. For instance the rate constant for the DNA polymerase dissociation process (k_{off}) is characterized by the *"waiting time"* prior to dissociation (τ_{ON}) and hence $k_{off} = 1/\tau_{ON}$. Lifetimes of the KF(exo$^-$) association and dissociation processes derived from the ion current recording shown in Figure 2a are τ_{OFF} = 12.1 s and τ_{ON} = 1.68 s in the presence of 7.4 nM of KF(exo$^-$)in the *cis* chamber. This gave the association and dissociation rate constants of $k_{on} = 1.12\times10^7$ $M^{-1}s^{-1}$ and $k_{off} = 0.60$ s^{-1}. In our experiment a pulling force is constantly exerted on the thread during ion current recordings because of the applied electric field, the induced electric force facilitated the dissociation of KF(exo$^-$) from the dsDNA segment of the rotaxane. This resulted in a larger k_{off} rate constant, and hence a larger dissociation constant ($K_d = k_{off}/k_{on}$ where higher K_d represents lower affinity) as compared to numbers found in the literature.

Table 1 | Comparison of KF rate constants

	Current work	Ref. 16a	Ref. 16b
DNA pol.	KF(exo$^-$)	KF	KF(exo$^-$)
Method	Nanopore Rotaxane System	Rapid Quench-Flow	QCM*
k_{on} ($M^{-1}s^{-1}$)	1.1×10^7	1.2×10^7	1.0×10^6
k_{off} (s^{-1})	0.60	0.06	3×10^{-3}
K_d (nM)	54	5.0	9.0

* QCM = Quartz crystal microbalance

- **Features of rotaxane *I/V* curves depend on DNA primer length (Supporting Figure2)**

The αHL•DNA-PEG^{phos} rotaxane presented here can be viewed as a single-molecule device that sets up a correlation between the observed ion current and the relative position of PEG^{phos} within the αHL protein nanopore. Translocation of the thread within αHL should lead to changes in recorded ion current with a properly designed and assembled rotaxane, as explained in the main text. Four rotaxanes were constructed and characterized to establish the correlation between ion current and thread spatial arrangement using DNA primers **P(0)**, **P(+3)**, **P(+5)**, and **P(+7)**, which are 24, 27, 29, and 31-nucleotides (nt) in length. The goal was to use these rotaxanes to mimic the translocation of the thread through αHL in discrete steps of 3, 2, and 2 nucleotides.

The I/V curves of these rotaxanes all manifest a characteristic deflection. Both the potential range of the deflections and the ion current at a certain applied potential have the order of **P(+7)** > **P(+5)** > **P(+3**) > **P(0**). These trends were interpreted based on the fact that the DNA and PEG^{phos} segments that make up the thread backbone differ in two ways: 1) The DNA is a polymer of deoxynucleotide monophosphates (dNMPs). The dNMPs which occupy a larger cross sectional area than the PEG^{phos} monomers (hexaethyleneglycol phosphate); and 2) The DNA segment has a higher charge density than PEG^{phos}, measured by the number of phosphate groups per unit length in the longitudinal direction. The DNA and PEG^{phos} segments has one negative charge (phosphate group) per 3.4 Å and 9 Å, respectively. We reasoned that a rotaxane with high PEG^{phos} to DNA ratio within the nanopore should block the αHL central channel to a lesser extent, and therefore the measured ion current should be **P(+7)** > **P(+5)** > **P(+3**) > **P(0**) under the same applied potential. On the other hand, higher PEG^{phos}/DNA ratio within the nanopore means that less force is exerted on the thread because the induced force under the influence of electric field is proportional to the number of backbone charges ($F = QE$). Furthermore, the energetic barrier that has to be overcome for entry and confinement of the dsDNA segment within the αHL vestibule is similar for all rotaxanes. Therefore a higher applied potential is required for a rotaxane constructed with a longer DNA primer to assume configuration ***B***, and hence the potential regions where the deflections appear have the order of **P(+7)** > **P(+5)** > **P(+3**) > **P(0**).

- **The deflection region of rotaxane *I/V* curves correspond to rapid fluctuation between configurations *A* and *B* (Supporting Figure 3)**

As noted in the main text, under positive potentials the rotaxane can adopt one of the two limiting configurations ***A*** or ***B***. The more etnergetically stable configuration ***A*** predominates at relatively low applied potentials while low force is exerted on the thread, where the dsDNA segment remains on the outside butting against the *cis* opening of αHL. On the other hand, the less energetically less favorable configuration ***B*** predominates at relatively high applied potentials, where the larger electric force exerted on the thread serves to overcome the barrier for dsDNA entry and confinement inside the αHL vestibule. The deflection region of the measured rotaxane *I/V* curves simply correspond to the range of applied potential where the exerted force does not bias the rotaxane toward either configuration ***A*** or ***B***, and within this potential range the rotaxane is expected to be metastable and fluctuate rapidly between the two configurations. This assumption was verified by obtaining an *I/V* curve of fine potential scanning at ΔV = 1 mV steps.

- **Attribute the new ion current level to DNA polymerase binding (Supporting Figure 4)**

In the real-time recordings we observed repeated occurrence of spikes at a consistent ion conductance level higher than the baseline, and these spikes appeared only after the addition of KF(exo$^-$) to the *cis* chamber. The new conductance level was tentatively assigned as configuration ***C***, corresponding to DNA polymerase binding to the dsDNA segment of the rotaxane. This notion was tested by introducing an excess amount of primer-template (P/T) complexes into the *cis* chamber to compete with the rotaxane for KF(exo$^-$) binding. A 42-nt ssDNA template **T** (an oligonucleotide that bears the same sequence as the DNA segment of the thread) was added to the *cis* chamber to hybridize to the existing $\mathbf{P^{dd}(0)}$ strands, which present a thousand-fold excess of P/T complex relative to KF(exo$^-$) (ratios between the amounts of P/T, KF(exo$^-$), and rotaxane are 10^{12}:10^9:1), and indeed the presumed single-molecule DNA polymerase binding events vanished soon after the addition of **T**.

- **Optimal applied potentials for monitoring DNA polymerase binding and function using the rotaxane system (Supporting Figures 5 and 6)**

The ion current increments (ΔI) associated with DNA polymerase binding to the dsDNA segment of the rotaxane is proportional to the magnitude of the applied potential, on the other hand, the baseline ion current fluctuation remains fairly consistent. Therefore higher signal to noise (S/N) ratio can be achieved simply by recording at higher applied potentials. However, this approach for boosting S/N will exert greater force on the thread, and thus has least two undesired effects. 1) The dsDNA segment becomes less accessible to DNA polymerase and result in reduced frequency of binding events; 2) At higher applied potentials, the environment deviates further away from the force-free condition that a DNA polymerase typically experiences, as is evident from the overall shorter binding event durations. Ion current recordings were obtained at selected potentials between +25 and +50 mV. It was found that +35 mV is optimal for real-time recording of KF(exo$^-$) binding and function using a rotaxane furnished with a 24-nt DNA primer $\mathbf{P^{dd}(0)}$ in the standard configuration (Supporting Figure 5).

The same considerations applies to a rotaxane assembled in the "reversed" configuration (Supporting Figure 1). Comparatively, a revered rotaxane cannot adopt the analogous configuration ***B*** because the αHL stem is too narrow for dsDNA entry, as a result the *I/V* curves of the reversed rotaxanes do not display a deflection region and the ion current increments (ΔI) resulting from to KF(exo$^-$) binding events are also smaller. Moreover a reversed rotaxane is considerably less stable than a standard rotaxane. This may be due to the fact that a reversed rotaxane cannot adopt configuration ***B***, which presumably stabilizes the dsDNA segment to some extent by preventing DNA primer dissociation from the thread. Consequently, ion current recordings can only be carried out within a narrow range and at lower applied potentials, where +25 mV was found to be optimal for experiments employing a rotaxane assembled using αHL, DNA-PEG^{phos} thread, and DNA primer **P(0)** (Supporting Figure 6). Recordings with the "reversed" rotaxanes were presented at the same ion current scale (y-axis) for comparison.

- **DNA polymerase binding and catalytic activity monitored in real-time (Supporting Figures 7-10)**

More ion current recordings are shown here in order to establish this supramolecular rotaxane system as a generalizable single-molecule technology. Supporting Figure 7 shows DNA polymerase binding events monitored using a rotaxane constructed with an all-DNA thread, as well as binding events by $9^{o}N_{m}$ and the large fragment of *B. stearothermophilus* DNA polymerase. Supporting Figure 8 shows more ion current recordings of KF(exo^{-}) binding and primer extension events. Supporting Figure 9 shows DNA binding and primer extension events carried out by KF(exo^{+}) and the *E. coli* DNA polymerase I protein. Supporting Figure 10 shows more ion current recordings of KF(exo^{-}) acting on a rotaxane in the "reversed" configuration.

In these figures, only selected sections of the whole ion current recording are shown. In Supporting Figure 8-10 the selected sections center around DNA polymerase-catalyzed dNTP incorporation events, and each non-productive binding event is marked by an asterisk. The duration of an experiment is denoted at the upper left corner of each panel, where time zero is defined by the moment when dNTP is added and the final identifiable incorporation event defines the end. If not noted otherwise, experiments were performed with a rotaxane constructed using αHL, DNA-PEG^{phos} thread, and DNA primer **P(0)** in a buffer solution containing 150 mM KCl, 25 mM Tris, 4.5 mM $MgCl_2$ at pH 7.5 (22 ± 2 ^{o}C) under an applied transmembrane potential of +35 mV. Ion current traces were all recorded at a sample rate of 10 kHz or higher, then filtered and presented at 50 Hz. For a primer extension events where more than one dNTP molecule was incorporated, the length of the resulting extended primer was inferred from the measured ion current of a series of rotaxanes assembled with every DNA primer with lengths between 24 and 31-nt (ref. 4) (Supporting Figure 2).

- **The relationship between temporal and spatial resolution (Supporting Figure 11)**

Noise is an intrinsic component of the output signal in any type of single-molecule measurement. Consequently the crude data often needs to be filtered and/or averaged before useful information can be obtained. While averaging enhances the signal to noise (S/N) ratio by canceling out random noise, temporal resolution is compromised. Here we offer a way to quantify and illustrate this relationship. First, we estimate the spatial resolution of a rotaxane system assembled using αHL, thread, and DNA primer **P(0)** in the standard configuration (Supporting Figure 1). Based on data obtained across multiple experiments, it was concluded that *on average* each nucleotide incorporation causes the ion current to increase by ~150 fA (ref. 4) (Supporting Figures 8 and 9). By assuming that the thread shifts 3.4 Å per nucleotide incorporation event (base stacking distance in B-form DNA), a distance-to-current conversion scale of $\Delta L/\Delta I \approx 22.7$ Å/pA can be established. We then approximate noise by calculating the standard deviation (σ) of the baseline. Here we report the resolution as the minimal ion current difference that can be distinguished at 95% confidence ($\pm 1.96\sigma$), and finally this number (ΔI) is translated into distance, and hence spatial resolution, using the $\Delta L/\Delta I$ conversion scale.

For example, the ion current recording shown in Supporting Figure 11e is presented at 20 Hz, and the baseline noise (σ) is 24 fA. This suggests that when the ion current increases (or decreases) by more than 94 fA (= 2 × 1.96 × 24 fA), it can be stated with at least 95% confidence that the change is *not* caused by random noise. Alternatively we can say that such change has *likely* arisen from a meaningful physical or chemical event, such as DNA polymerase binding or primer extension. The spatial resolution can then be estimated according to the $\Delta L/\Delta I$ conversion scale, in which ΔI = 94 fA is equivalent to ΔL = 2.1 Å. However, at this temporal resolution/sample rate (20 Hz), events lasting less than 1/20 seconds would be smoothed out by averaging and cannot be unequivocally identified. It should be noted that although the above analysis regarding the inverse relationship between spatial and temporal resolution is general to any single-molecule observation technique, the actual numbers for the present rotaxane system should be cited with caution since noise and ΔI are dependent on many factors, ex. chemical structure of thread, sequence of DNA primer, composition of buffer, rare heterogeneity of the αHL protein, etc.

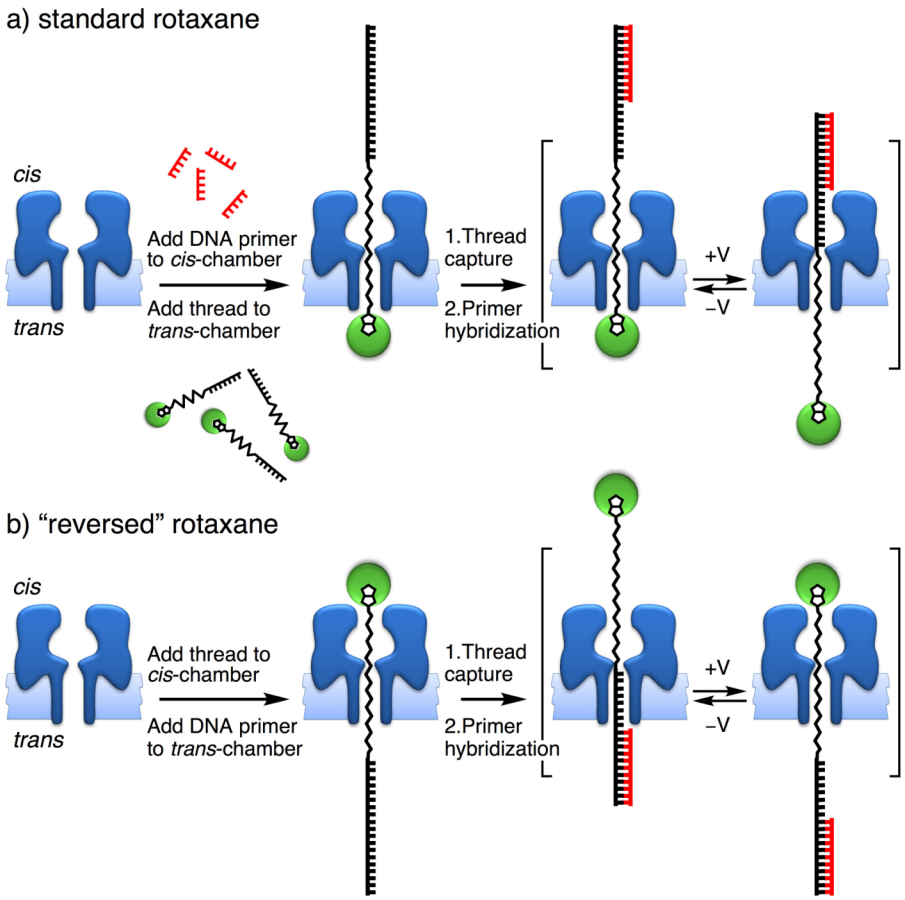

Supporting Figure 1 | Construct a supramolecular αHL•DNA-PEG^{phos} rotaxane architecture. a, To prepare a rotaxane in the standard configuration, DNA primer of desired sequence and length and the streptavidin-capped DNA-PEG^{phos}-biotin hybrid thread were added to the *cis* and *trans* sides of a single αHL embedded within an artificial planar lipid bilayer. An applied potential of –125 mV (or more, *cis* side defined as the ground) proved sufficient for the capture of the thread, which was reflected by a characteristic decrease in ion current to approximately –5 pA in a 150 mM KCl buffer solution at pH 7.5. The applied potential was then lowered to –40 mV to allow primer access to the 3’-DNA segment of the thread exposed in the *cis* chamber. **b**, To prepare a rotaxane in the “reversed” configuration as shown above, the same procedure as in **a**, was followed, except that DNA primer of desired sequence and length and the streptavidin-capped DNA-PEG^{phos}-biotin hybrid thread were added to the *trans* and *cis* sides, respectively.

NOTE: The DNA-PEG^{phos}-biotin•streptavidin complex was prepared by mixing the two components at a 1:4.1 (or higher) molar ratio to ensure that all four biotin binding sites of the streptavidin were occupied. The mixture was then directly used in our experiments without further purification. For clarity here the streptavidin was shown to be bound by only one thread strand.

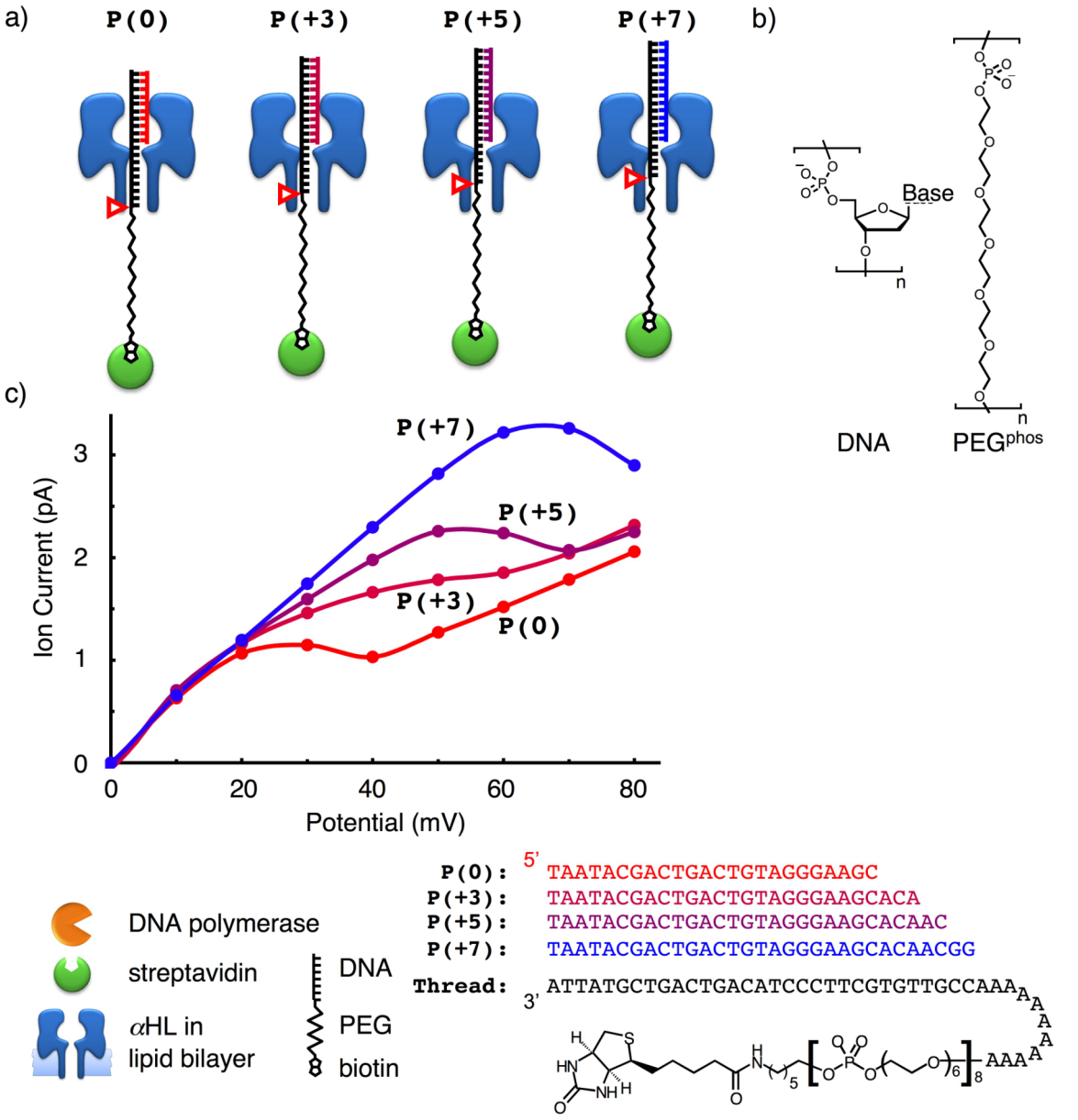

Supporting Figure 2 | *I/V* curves of rotaxane constructed with various length of DNA primers. The *I/V* curves shown here is taken from ref. 4. The sequence and structure of the thread and DNA primers used to construct the rotaxanes characterized in this experiment are shown at the bottom. All DNA are named according to their relative lengths to the 24-nt strand **P(0)**. **a**, A rotaxane constructed with a longer DNA primer will have a higher PEG^{phos}/DNA ratio within the stem portion of αHL. **b**, The monomer unit for PEG^{phos}, as compared to that of DNA, has smaller cross sectional area and less phosphates per backbone unit length in the longitudinal direction. **c**, Here we compare the *I/V* curves measured for rotaxanes assembled using the same thread but different DNA primers 24, 27, 29, and 31-nt in length [**P(0)**, **P(+3)**, **P(+5)**, and **P(+7)**]. The two expected trends among this series of rotaxanes were verified. Rotaxane with a longer primer will manifest 1) a higher ion current under the same applied potential; and 2) a higher deflection potential range in its *I/V* curve. Both trends appear in the order of **P(+7)** > **P(+5)** > **P(+3)** > **P(0)**.

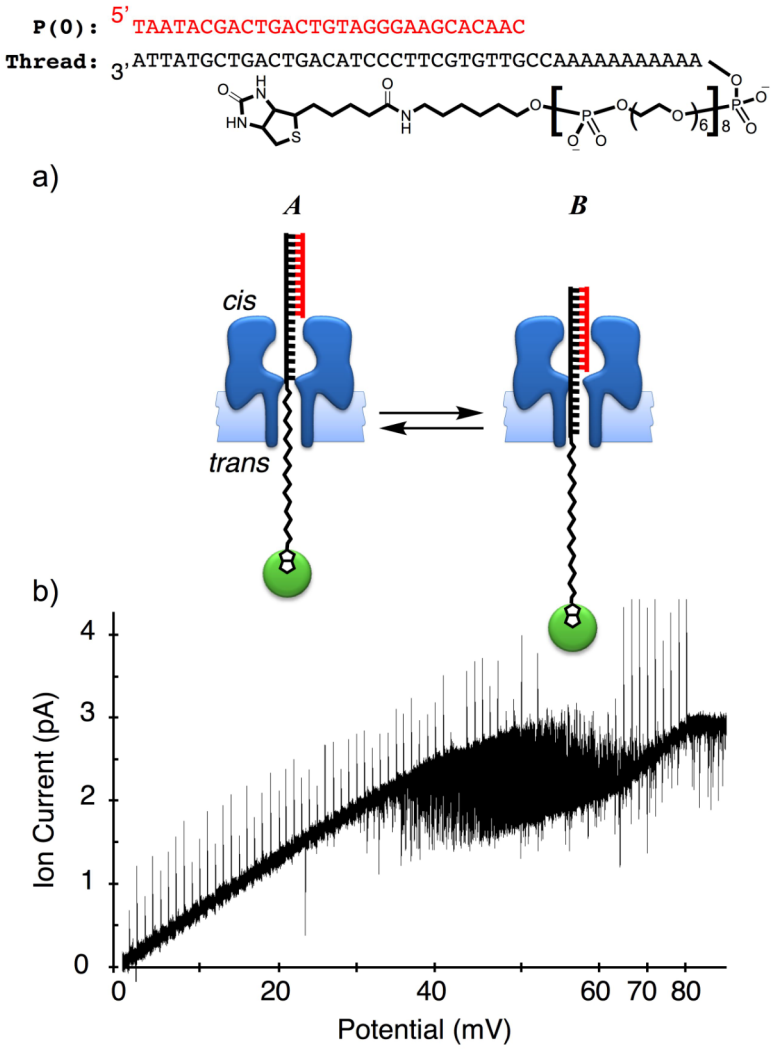

Supporting Figure 3 | Rotaxane fluctuates rapidly between configurations *A* and *B* in the *I/V* curve deflection region. In this experiment we employed a rotaxane constructed with the thread and a 24-nt DNA primer **P(0)**; their structure and sequence are shown at the top. **a**, As discussed in the main text, the rotaxane can adopt either configuration ***A*** or ***B*** depending on the magnitude of the applied potential. At relative low potentials the more stable configuration ***A*** is expected to predominate; the rotaxane can adopt configuration ***B*** when relatively high potentials is applied to overcome the unfavourable energetic requirements of dsDNA entry and confinement within the αHL. **b**, Here we performed fine potential scanning by ΔV = 1 mV steps to fully characterized the potential dependence of the rotaxane configuration. We expected, and verified, that within the deflection region of the *I/V* curve, the rotaxane rapidly fluctuates between configurations ***A*** and ***B*** since the force exerted on the rotaxane is not sufficient to completely bias it toward either configuration.

NOTE: Sodium chloride (150 mM NaCl) was used as the major salt component in the buffer to perform the experiment shown in **b** as NaCl is known to amplify noise in the deflection region. The enhanced noise in the deflection region is not obvious to the naked eye in standard KCl buffer in which these experiments were carried out.

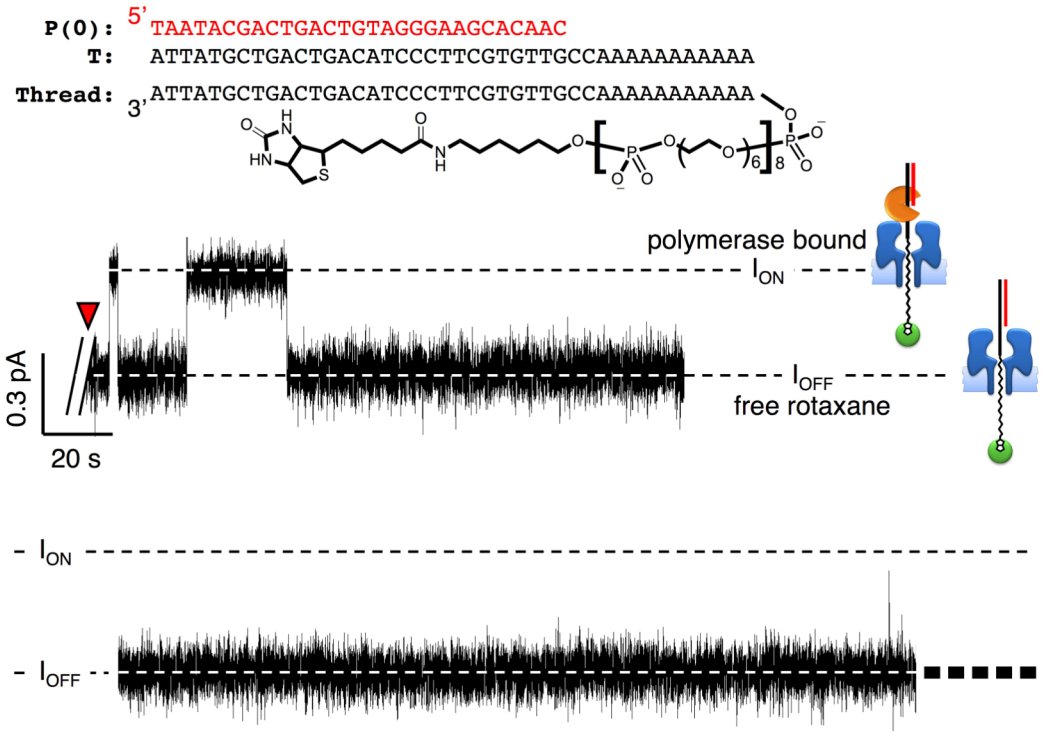

Supporting Figure 4 | DNA polymerase binding to the rotaxane dsDNA segment induces the higher ion current level. Here we show a negative control experiment conducted immediately after the recordings of DNA polymerase binding events shown in Figure 2. The sequence and structure of the thread and DNA primer used to construct the rotaxane employed in this experiment are shown at the top The red pointer marks the addition of the DNA template strand (**T**) bearing the same sequence as the 3'-terminus of the thread to the *cis* chamber, while solution in the *cis* chamber already contained DNA primer **P(0)** added in the beginning of the experiment to form the rotaxane. Hybridization of **P(0)** and **T** formed primer/template (P/T) complexes that could compete with the dsDNA segment of the rotaxane for KF(exo$^-$) binding. The P/T complexes represented a thousand-fold excess (ratio between the amounts of P/T, KF(exo$^-$), and rotaxane is 10^{12}:10^9:1) and therefore should saturate all KF(exo$^-$) binding sites. As expected, no events were observed soon after the addition of (**T**), while bindings events (ion current spikes) occurred at a frequency of ~ 5 events per minute prior to the addition.

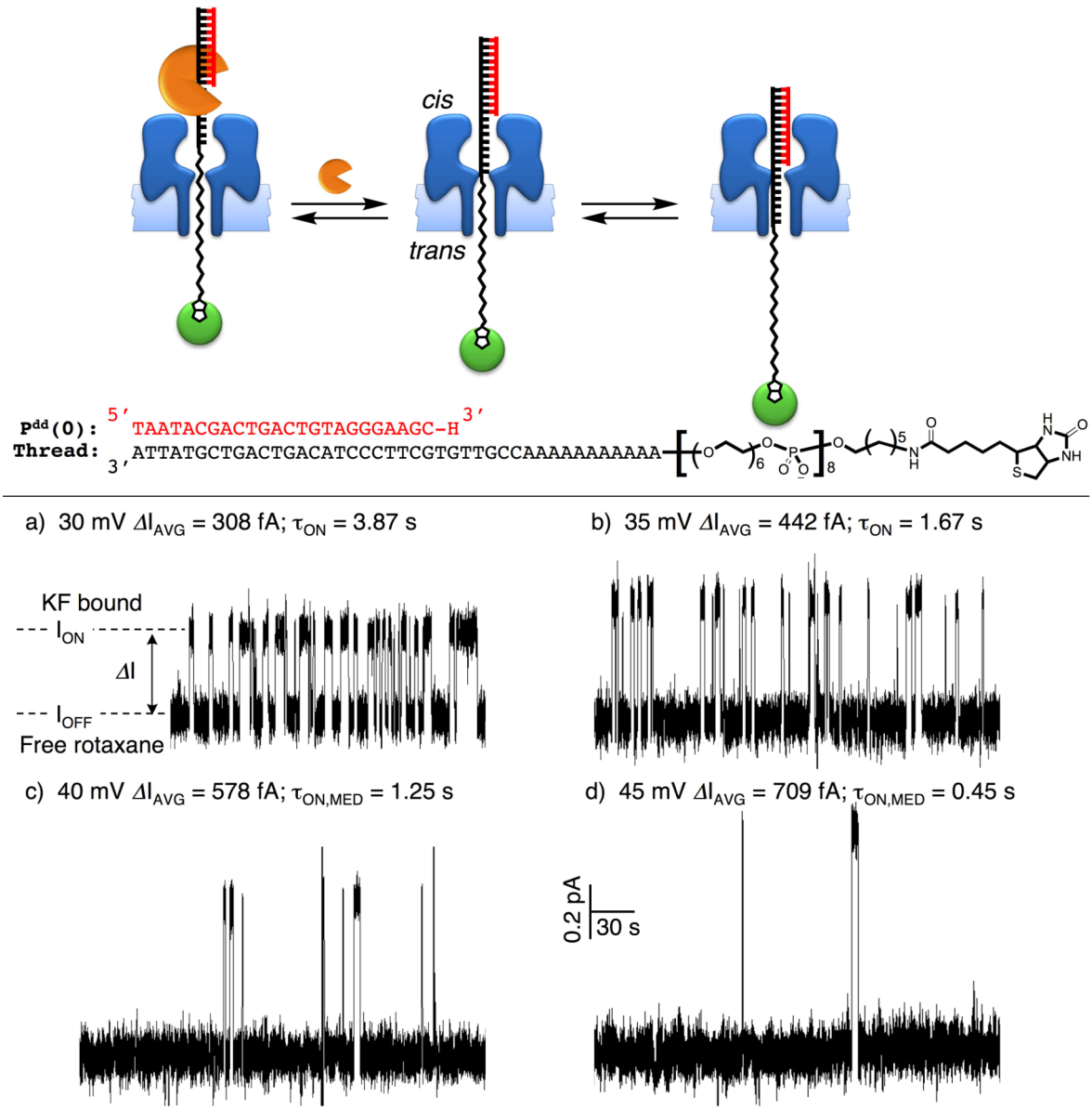

Supporting Figure 5 | Search for the optimal applied potential for monitoring KF(exo⁻) binding and function in real-time. Sequence and structure of the thread and dideoxy-terminated DNA primer used to construct the rotaxane are shown at the top. A section of each ion current trace recorded at **a**, 30 mV **b**, 35 mV **c**, 40 mV and **d**, 45 mV displaying multiple real-time single-molecule KF(exo⁻) binding events were shown. The total number of events observed over the full recording are 118, 224, 14, and 4, respectively. All recordings are presented at the same scales and at 50 Hz resolution. The ΔI resulting from KF(exo⁻) binding (and thus the S/N ratio) increased as the applied potential increased [ΔI = I (binding) – I (baseline)], on the other hand, the binding events became less frequent, and overall with shorter durations. In **a** and **b**, the τ_{ON} values were obtain by fitting exponential decay functions to the lifetime histograms (see Supporting Discussion regarding kinetic analysis), while simply the median event duration was reported in **c** and **d**, since there were not statistically relevant numbers of binding events recorded.

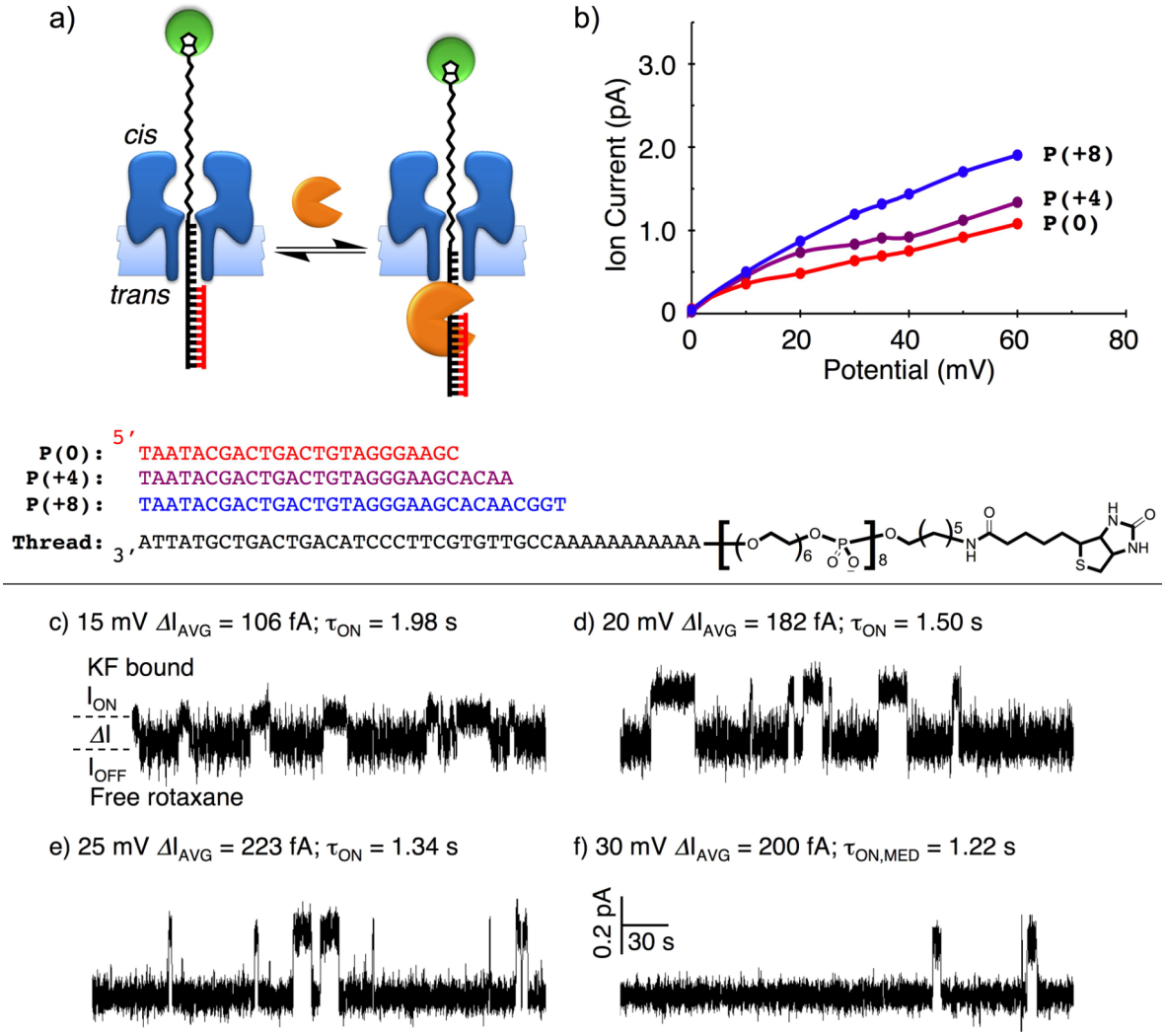

Supporting Figure 6 | Characterize a rotaxane assembled in the "reversed" configuration. Sequence and structure of the thread and DNA primers used to construct the "reversed" rotaxanes are shown at the top. See Supporting Figure 1b for procedures for constructing the these rotaxanes. **a**, KF(exo⁻) binding leads to higher PEG^{phos}/DNA ratio within the αHL and is associated with a higher ion conductance level. **b**, In this configuration the dsDNA segment cannot enter the stem of αHL, and therefore no pronounced deflection was observed in the measured *I/V* curves. A reversed rotaxane assembled using thread and DNA primer **P(0)** was employed to empirically determine the optimal applied potential for monitoring DNA polymerase binding and function. A section of each ion current trace recorded at **c**, 15 mV **d**, 20 mV **e**, 25 mV and **f**, 30 mV displaying multiple real-time single-molecule KF(exo⁻) binding events were shown. The total number of events observed over the full recording are 50, 69, 119, and 18, respectively. All recordings are presented at 50 Hz resolution and at the same scales as that in Supporting Figure 5 for comparison. Similar to rotaxanes in the standard configuration, the Δ**I** resulting from KF(exo⁻) binding (and thus the S/N ratio) increased as the applied potential increased, on the other hand, the binding events became less frequent, and overall with shorter lifetimes. In **c**, **d**, and **e**, the τ_{ON} values were obtain by fitting an exponential decay function to each binding event duration histogram (*vide infra*), while simply the median event duration was reported in **d**, since there were not statistically relevant numbers of binding events recorded. The reduced stability of rotaxanes in this configuration only allows ion current recordings at applied potentials ≤ 35 mV.

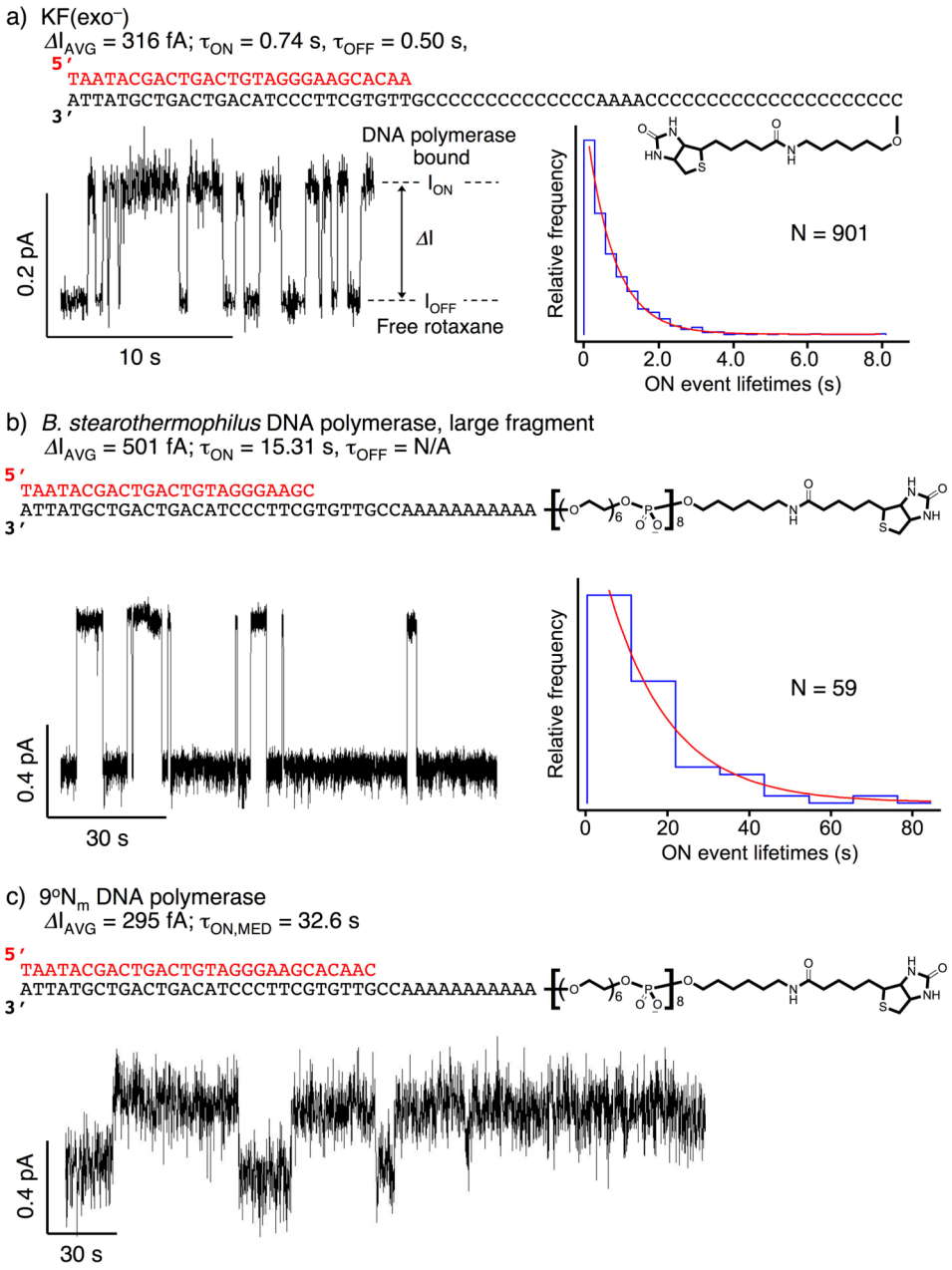

Supporting Figure 7 | Generality of the rotaxane system for monitoring DNA polymerase binding. In each panel, the sequence and structure of thread and DNA primer used to construct the rotaxane are shown at the top, and histogram of the ON event durations are shown at the right. **a**, KF(exo$^-$) binding to a rotaxane constructed with an all-DNA thread was monitored in real-time. **b**, Binding events of the Large fragment of *Bst* DNA polymerase; and **c**, 9°N$_m$ DNA polymerase were monitored in real-time. In **b**, analysis of the off events did not give satisfactory τ_{OFF} fitting, likely because there was not sufficient number of recorded events. In **c**, the crude ion current recording was filtered and presented at 10 Hz. Simply the medium binding event duration was reported since the number of binding events recorded was not statistically relevant to obtain τ_{ON}.

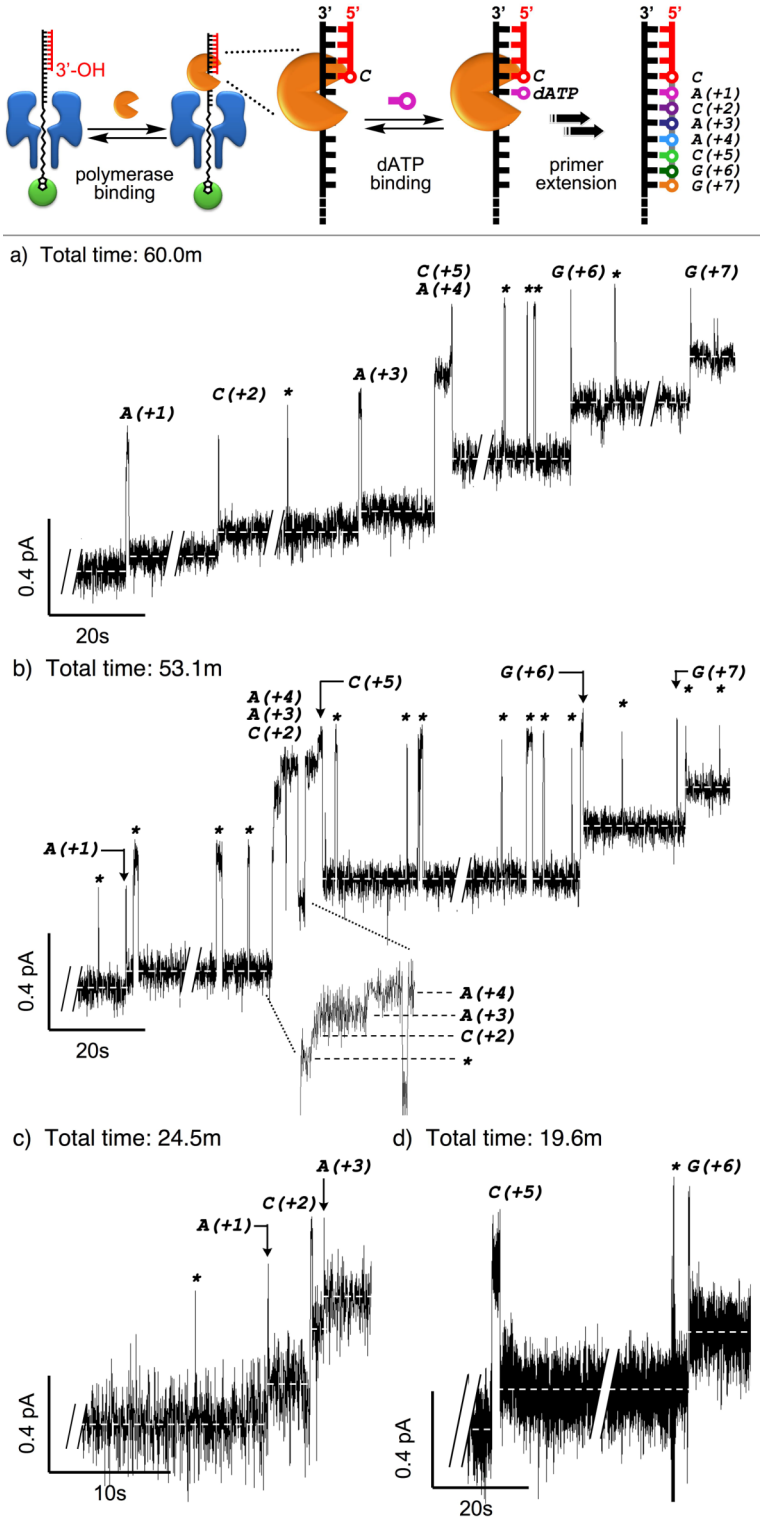

Supporting Figure 8 | More ion current recordings showing real-time KF(exo$^-$) binding and DNA primer extension events. Asterisks denote non-productive DNA polymerase binding events. Experiments were performed under standard conditions (*vide supra*), with the exception of **b**, the α-thio-analogue of deoxycytidine triphosphate (dCTPαS) was used instead of dCTP. **d**, the starting DNA primer was **P(+4)** instead of **P(0)**.

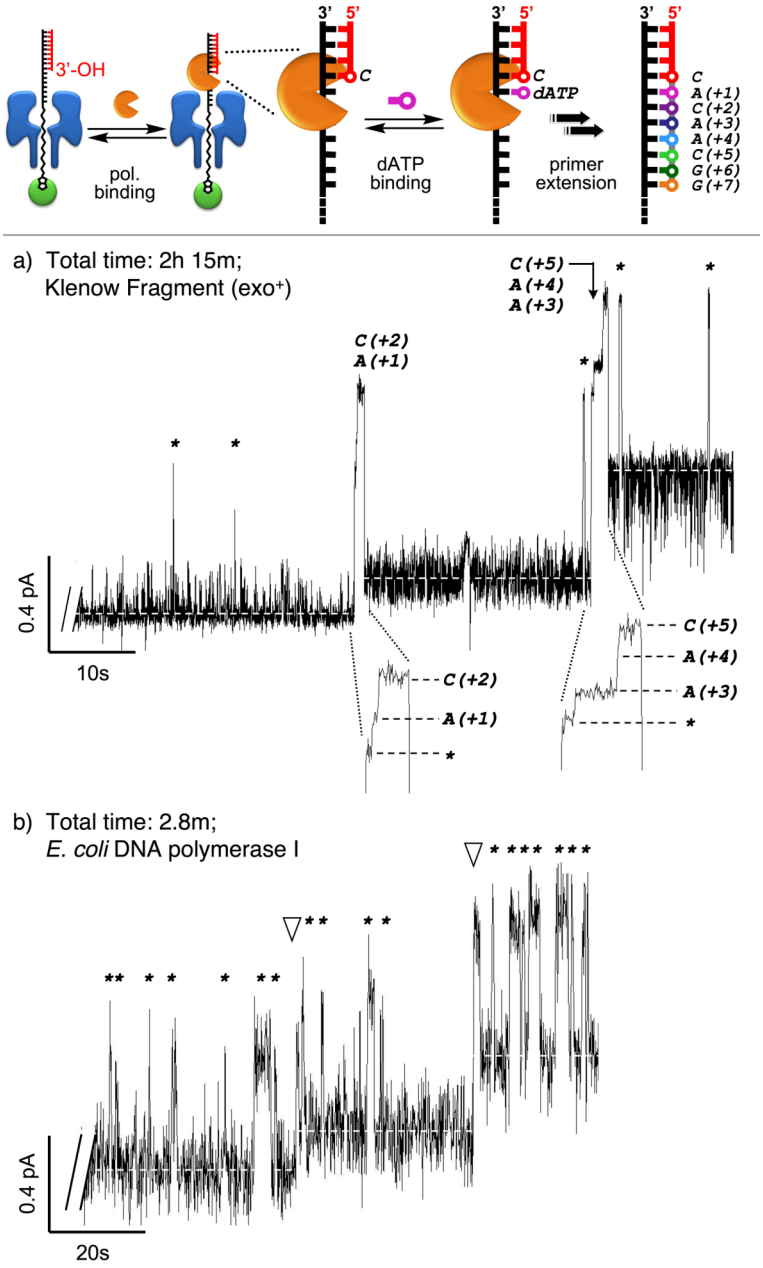

Supporting Figure 9 | Ion current recordings showing real-time binding and primer extension events of DNA polymerase other than KF(exo⁻). Asterisks denote non-productive DNA polymerase binding events. Experiments were performed under standard conditions (*vide supra*), the only exception is that in **b**, *E. coli* DNA polymerase I was employed and the ion current recording was filtered and presented at 10 Hz. The noise during ion current recording was higher than usual due to hardware issues unrelated to the intrinsic properties of the enzyme. An incorporation event is marked with an inversed open triangle when the length of the resulting extended primer cannot be unequivocally identified.

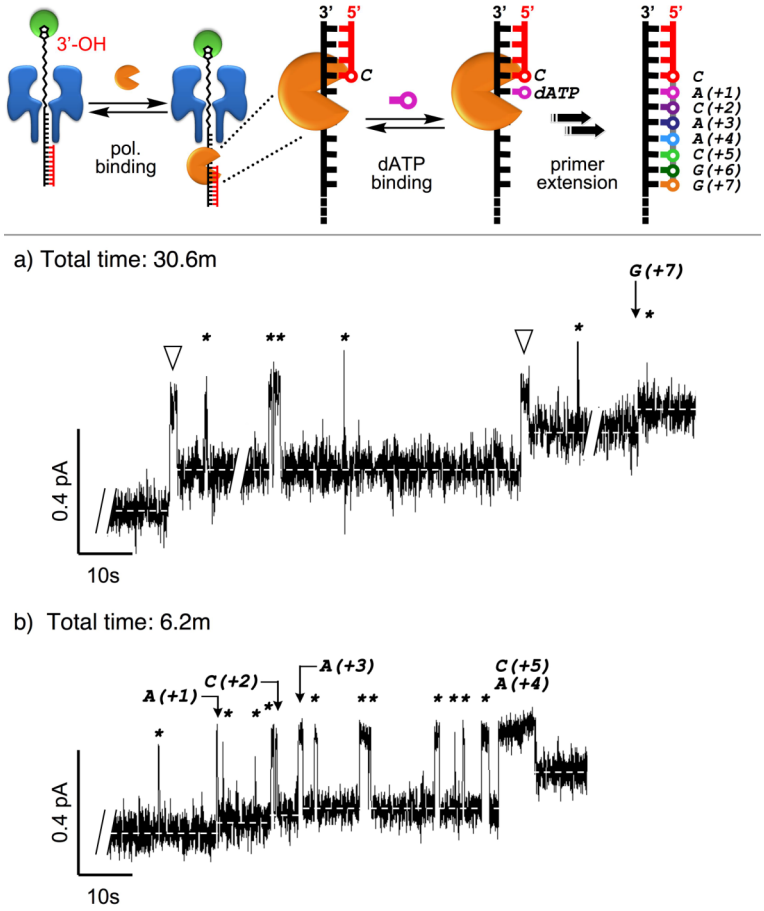

Supporting Figure 10 | Ion current recordings of real-time KF(exo⁻) binding and primer extension events performed on rotaxanes in the "reversed" configuration. Asterisks denote non-productive DNA polymerase binding events. Ion current recordings were done at an applied potential of +25 mV because rotaxanes in this configuration are generally less stable (see Supporting Figure 6). Both ion current traces were filtered and presented at 25 Hz. An incorporation event is marked with an inversed triangle when the length of the resulting extended primer cannot be unequivocally identified.

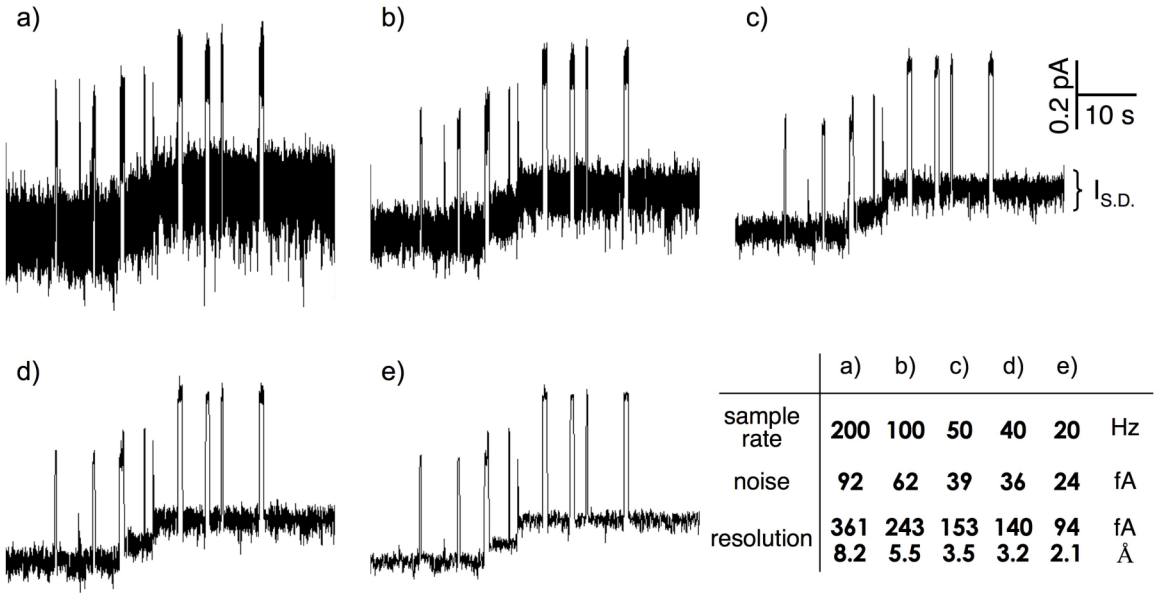

	a)	b)	c)	d)	e)	
sample rate	200	100	50	40	20	Hz
noise	92	62	39	36	24	fA
resolution	361	243	153	140	94	fA
	8.2	5.5	3.5	3.2	2.1	Å

Supporting Figure 11 | Spatial resolution vs. temporal resolution. The series of ion current recording shown here displays the first two single-nucleotide incorporation events shown in Figure 3b in the main text. Here we referred to the sampling rate (*i.e.* temporal resolution) as the final data density that was presented, where all of the raw data in this manuscript were recorded at 10 kHz or higher. For example the original recording for this figure was sampled at 20 kHz, filtered, and then presented at **a**, 200 b, 100 **c**, 50 **d**, 40 and **e**, 20 Hz. Noise was quantified by the standard deviation (σ) of the baseline ion current fluctuation ($I_{S.D.}$) and the resolution achievable at 95% confidence for each sample rate is summarized in the lower right table. Resolution in terms of ion current is simply $2 \times 1.96 \times \sigma$, and the spatial resolution is obtained by referring to the distance-to-current conversion scale (see Supporting Discussion for more details).